AIAA SciTech Forum
8-12 January 2024, Orlando, FL
AIAA SCITECH 2024 Forum

10.2514/6.2024-2691

Active Charge Control Using an Electron Beam and Ultraviolet Light Source

James D. Walker III* and Hanspeter Schaub†
Department of Aerospace Engineering Sciences, University of Colorado Boulder, Boulder, Colorado

The development of active charge control techniques is an important step for testing and implementing electrostatic actuation methods, such as debris removal with the Electrostatic Tractor. A proportional and derivative (PD) controller is developed and applied to a system consisting of a high energy electron gun and VUV lamps in order to achieve this. The PD controller maintains a desired potential on the target by limiting the amount of current emitted from the electron gun. Using experiments in a vacuum chamber, it is found that, for a variety of charging scenarios, the control achieves the desired potential with a steady state error less than 3% across all configurations. Further, the discharging behavior is explored, demonstrating the need for the photo-electric current generated by the VUV lamps for the controller to converge in a reasonable amount of time. It is discovered that the electron beam can be used to discharge the target object, however, this would require electron beam energy control rather than current control.

I. Introduction

When exposed to the energetic plasma environment of space, electrons and protons impact and accumulate on the surface of spacecraft[1]. These interactions cause the surface of spacecraft to acquire electrostatic potentials[1]. Satellites are especially vulnerable to this charging behavior in geostationary (GEO) and cislunar orbits because these regions have a large flux of high energy electrons causing spacecraft potentials to exceed thousands of volts[1]. As charged objects approach one another, the electrostatic forces between then become significant and can impact a spacecraft's relative motion[2–4]. These electrostatic forces have the most impact on relative motion when the separation distance between the two spacecraft is small, specifically during proximity and rendezvous operations[2, 3]. Risk of electrostatic discharges (ESDs) also arise during docking operation: if two spacecraft with different electrostatic potentials come in contact, this potential difference can cause an ESD event and damage the spacecraft[4].

While there have been reasons presented for reducing and eliminating the effects of spacecraft charging, they also offer unique capabilities for debris removal. If the electrostatic forces are controlled, a servicing spacecraft would be able to contactlessly apply a force to a target object. The Electrostatic Tractor (ET) is a novel method for active debris removal in geostationary orbits that utilizes these electrostatic forces [5, 6]. Equipped with a high energy electron gun, a servicing spacecraft directs a beam of electrons at the target, imparting a negative current and decreasing the potential on the target [6]. Because the servicing craft is losing electrons, it experiences a positive current and an increasing potential[6]. By driving the target to a negative potential and the servicer to a positive potential, an attractive Coulomb force is generated between them[6]. Using low impulse thrusters, the servicing craft is capable of "tugging" the debris object to a new, graveyard orbit, eliminating the danger it poses in GEO orbit[7, 8]. A concept of this process is shown in Fig. 1. It was found that using the ET, a servicing craft can can re-orbit a multi ton debris object in a matter of months [9].

For the ET to be properly implemented, the servicing craft must be capable of actively controlling the Coulomb force by controlling the spacecraft potentials. The electron gun applies a negative current to the target, but, for effective control, the servicer must also apply a positive current. If not, when the servicer drives the target slightly too negative, it cannot correct the error. A positive current can be generated using vacuum ultraviolet (VUV) lights. High energy photons impact and induce a photo-electric effect on the surface of target, causing electrons to be emitted from the surface of the spacecraft[1]. This emission of electrons acts as a positive current on the target. However, simply applying

*Graduate Research Assistant, Ann and H.J. Smead Department of Aerospace Engineering Sciences, University of Colorado Boulder, Colorado Center for Astrodynamcis Research, Boulder, CO, 80303 USA. James.WalkerIii@colorado.edu

†Professor and Department Chair, Schaden Leadership Chair, Ann and H.J. Smead Department of Aerospace Engineering Sciences, Colorado Center for Astrodynamics Research. AAS Fellow, AIAA Fellow

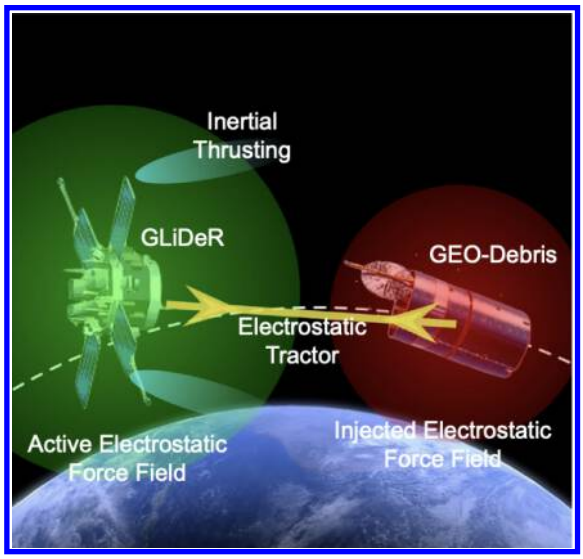

Fig. 1 Conceptual representation of two charged spacecraft connected by Electrostatic Tractor[6].

both currents is not sufficient, there must be a controller that maintains the desired potential. This requires active charge control; "active" referring to the use a feedback controller.

Previous methods for active charge control have mainly employed the use of ion emitters to maintain electric potentials close to 0 V[10–14]. This is useful for satellites orbiting in Earth's magnetosphere [12–14]. Regions of the magnetotail lobes can impart up to +70 V on the surface of the spacecraft which will interfere with the electric field and low energy electron and ion flux measurements taken by the satellite[12, 14]. Ion emitters as well as electron beams have also been investigated for active charge control for Coulomb spacecraft formations[15]. Similar to the ET described above, by maintaining desired electrostatic potential on each spacecraft in a formation, the Coulomb forces between the formation can be used to control the satellites relative motion[15]. As shown by the previous research, active charge control has mainly been investigated for a spacecraft to control its own electric potential, not the potential of a target. The idea of controlling a target's electrostatic potential has been discussed, specifically in terms of the ET; however it has not yet been investigated experimentally[5, 6].

This paper focuses on the development and implementation of active charge control of a target's potential in a vacuum chamber environment. A vacuum chamber environment is an ideal environment for charge control experiments due to rapid measurement capabilities and lack of plasma currents experienced by spacecraft. If active charge control cannot be achieved in this environment, it would be extremely difficult to achieve in a more realistic environment. Instrument requirements, specifically vacuum ultraviolet lights, are investigated with experimental results. Additional control techniques are also addressed. The implemented control varies the output current of the electron gun, but the energy of the emitted electrons can be controlled as well. While the idea is explored, energy control is not implemented in this paper.

Section II details the underlying physics of the effect of the electron beam and VUV lights as well as the implementation of the PD controller. Section IV describes the experimental setup for this project. Experimental data and an explanation of the results is presented in Section V and is outlined as follows: floating potential experiments are conducted first to determine the maximum potential achievable for each beam energy. Next, the capabilities of active charge control are explored for a variety of beam energies and goal potentials. In the final two subsections, discharging behavior is explored, first using VUV lamps then using just the electron beam at varying energies.

II. Overview of Numerical Charge Modeling

In order to fully control the electrostatic potential of a target, the servicing spacecraft must be capable of applying both a positive and negative current. The electron beam emits a stream of energetic electrons that impact and stick to the target, generating a negative current. This current only occurs when the difference in electric potential between the servicer ϕ_S and the target ϕ_T is less than the initial energy E_{EB} of the electron beam. When the difference is greater than or equal to the electron beam energy, the emitted electrons do not have enough energy to reach the target and are

deflected away. This is current is expressed by

$$I_T(\phi_T) = -\alpha I_{EB} \qquad \phi_S - \phi_T < E_{EB} \tag{1a}$$

$$I_T(\phi_T) = 0 \qquad \phi_S - \phi_T \geq E_{EB}, \tag{1b}$$

where the current of the electron beam is I_{EB} and α is the fraction of the beam hitting the target. Assuming an accurate and focused beam, $\alpha = 1$, such that $I_T = -I_{EB}$ if the beam reaches the target.

Impacting electrons can also generate positive currents caused by the emission of secondary and backscattered electrons[1]. When an electron impacts the surface of an object, if it has enough energy, the impacting electron will interact and share energy with the surface electrons[1]. When enough energy is transferred to a surface electron, it can be be emitted from the material as a secondary electron[1]. This electron emission applies a positive current to the target object. Because this secondary electron current is caused by impacting electrons, its magnitude is proportional to the electron beam current. However, the probability of a secondary electron emission is a material property and is described as the ratio of outgoing to incoming electrons, referred to as the secondary electron yield (SEY) and denoted as $\delta(E)$[1]. This electron yield is dependent on the energy of the impacting (primary) electron, E, such that each material will have a characteristic SEY curve. Depending on the material and the beam energy, this ratio can be greater than 1, meaning the electron beam is actually applying a net positive current to the target[1]. The electron flux generated by the secondary electrons can be written as

$$J_{se} = \int_0^\infty \delta(E) f(E) E \, dE, \tag{2}$$

where $f(E)$ is the electron velocity distribution of the primary electrons[1]. Completing this integration gives the number of secondary electrons being emitted for a unit area[1], which in turn can be used to find the secondary electron current, I_{se}, for a given surface and time.

Backscattered electrons are similar to secondary electrons because they apply a positive current on the target due to electron "impacts". When an electron approaches a surface, it can be reflected, or backscattered, away[1]. This typically occurs around ion sites[1]. The backscatter yield, denoted $\eta(E)$, is a material property but also depends on incident angle and electron energy. Similar to Eq. (2), the electron flux of backscattered electrons is given in Ref. 1 as

$$J_{be} = \int_0^\infty \eta(E) f(E) E \, dE. \tag{3}$$

Similarly, Eq. (3) can be used to solve for the total backscattered electron current, I_{be}, for a given surface and time.

The secondary and backscattered electron yields ($\delta(E)$ and $\eta(E)$) are independent and can be added together to get the total electron yield[1], which is how these properties are often presented. Figure 2 shows the experimentally obtained total electron curve for poly-crystalline gold[16]. In this figure, σ_{max} refers to the maximum yield and $E_{\max}$ is the energy at which this maximum occurs. The first and second crossover energies, denoted E_1 and E_2 respectively are important properties. These value correspond to yield values of 1, where the incoming and outgoing electrons are equal and the electric potential is constant.

It can be seen that E_1 is an unstable equilibrium while E_2 is stable[1]. If a system is at E_1 it will remain there, but if it is slightly above or below, the system will be driven away: below E_1, there is a negative net current and driving the incident electron energy to 0 while above E_1, the current is positive, increasing the incident electron energy[1]. On the other hand, for E_2, if the system is slightly above E_2 the target potential will again be driven to 0, but when the system is below E_2, the incident electron energy will be driven to E_2[1]. This means that as long as an electron beam energy greater than E_2 is being applied, the target potential will be driven to a constant floating potential that occurs when the incident energy is at E_2. A more detailed explanation of this is given in Ch. 9 of Ref. 1.

VUV lights are also used throughout this project to generate a positive current on the target through the photo-electric effect. When a high energy photon impacts a surface, it can be absorbed by an electron, moving the particle to an excited state[1]. In order for an electron to be emitted, the absorbed photon must have a greater energy than the work function of the material[1]. Then, if enough energy is absorbed, the electron can be emitted, similar to secondary electrons. This emission of photo-electrons generates a positive current on the target. The photo-electron flux is detailed in Ref. 1 as

$$J_{ph} = \int_0^\infty Y(\omega) f(\omega) \, d\omega. \tag{4}$$

Equation (4) looks similar to Eqs. (2) and (3) with Y(ω) as the photo-electric yield of the material and f(ω) as the photon flux; however, Eq. (4) is integrated over the photon energy, ω[1]. As before, the total photo-electron current, I_{ph}, can be found for a specific time and surface area.

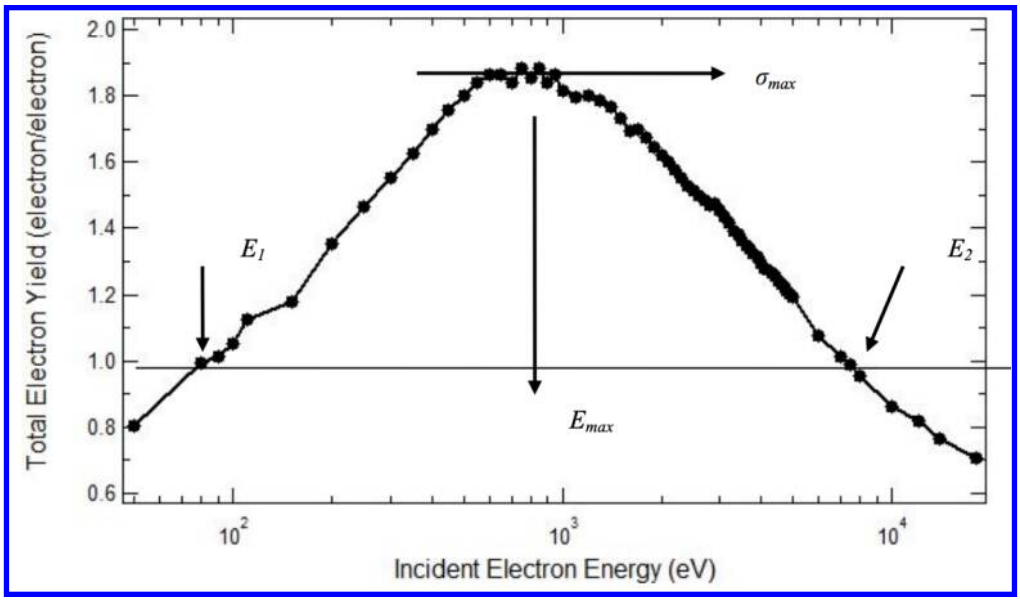

Fig. 2 The total electron yield of poly-crystalline gold as determined by Ref. 16. The first and second crossover energy are indicated by E_1 and E_2.

When all these currents are equal, the incoming and outgoing electrons will be equal, and the target potential will remain constant[1]:

$$I_{net} = -I_T + I_{se} + I_{be} + I_{ph} = 0 \tag{5}$$

This current balance will occur for a given equilibrium potential, in other words, the currents will only balance for specific target potentials. In Ref. 17, it was discovered that charging via an electron gun results in multiple equilibrium potentials that satisfy (5) depending on the target's initial potential. If a target starts at 0 V and is irradiated with an electron gun, the final potential will be different than if the target started a significantly negative value[17]. Throughout this paper, the charging scenarios presented start with the target at 0 V, meaning the second equilibrium will not be achieved. Results are presented for applying an electron beam current when the target has a negative charge, but the focus of the section is to compare the transient discharging behavior between the electron gun and VUV lights so the other equilibrium points are not considered.

For each of the charge control scenarios presented in this paper, a PD controller is used to drive the target potential to a desired goal potential. This is achieved by adjusting the electron beam current such that the equilibrium shown by (1) occurs when the target potential is the goal potential.

III. Target Voltage Control

A PD control is developed and applied to the grid of the electron gun. Typically, a controller requires a direct relationship between the input and output. In this case, it would be between the electron beam current and the target potential. The controller would determine the amount of current required to achieve the desired target potential and drive the electron beam current to that value. This relationship requires a balance of all the currents applied to the target described in the previous section. A major concern with finding this current balance is that it depends on yield models that can be inconsistent. Reference 18 surveys various secondary electron emission models for aluminum and demonstrates that different models yield significantly different results for secondary electron generation. These parameters also depend on parameters such as surface roughness and contamination layers that are difficult to estimate and model[19, 20]. Additionally, it was found that experimentally determined yields can vary day to day[21]. Rather than using this approach that depends on inconsistent models, an indirect relationship can be used. The electron beam current is controlled by the grid of the electron gun: when a voltage is applied to this grid, it limits the number of electrons that are emitted. Because of this, control can be implemented on to electron gun grid to control the electron beam current.

Two types of control are utilized in this paper: proportional (P) and derivative (D) control. The P control is

proportional to the error: a measure of the target's electric potential is taken using an electrostatic probe (detailed in the next section). The difference between the measurement and goal potential is the error. Equation (6) shows the proportional control, δV_P

$$\delta V_P = K_P(V_F - V_T) \tag{6}$$

where V_T is the measurement of the targets potential, V_F is the goal potential, and K_P is the proportional gain. The proportional gain can be adjusted to increase/decrease the strength of the control. To apply this control, δV_P is simply added to the current grid voltage. When the target potential is more positive than the goal and V_F - V_T < 0, the proportional control will be negative, decreasing the grid voltage and thereby increasing the electron beam current. The larger current will drive the target potential more negative, closer the the goal potential. When the opposite occurs and $V_F > V_T$, δV_P will be positive, resulting in a lower beam current. Once the target reaches its goal potential, the proportional control will be 0 and the beam current will be constant.

The other type of control applied is derivative control. This control is proportional to the rate of change of the error. To find this, the error measurement from the current step is subtracted from the previous error:

$$\delta V_D = K_D \frac{\delta V_{t-1} - \delta V_t}{dt}. \tag{7}$$

Similar to before, K_D is the derivative gain that allows for the strength of the controller to be adjusted, δV_t and δV_{t-1} are the error measurements at the current and previous time step respectively, and dt is the time between measurements. This control is added directly to the grid potential as well; for PD control, both δV_P and δV_D are added to the grid potential. When the difference in errors is large, the target potential is being driven toward the goal potential quickly, likely leading to an overshoot and an underdamped system. With derivative control, a large change in the error will result in large derivative control that acts opposite to the proportional control, slowing the change and reducing overshoots, allowing the system to converge to the control quicker.

IV. Experimental Setup

Experiments for this project are conducted in the JUMBO vacuum chamber at the Air Force Research Labs (AFRL). The experimental setup includes a Faraday cup, UV detector, electrostatic voltmeter (Trek Probe), and a 4 in diameter gold-plated copper disk. Figure 3 shows the experimental setup used throughout this paper.

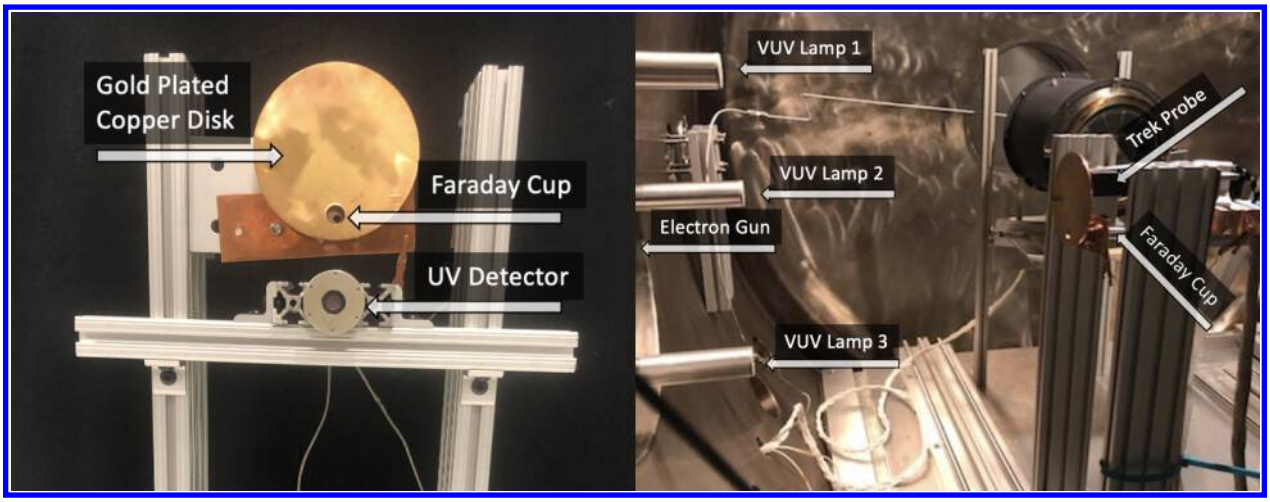

Fig. 3 The experimental setup used throughout this project. (Left) The portion of the setup directly exposed to the electrons beam and VUV photons. (Right) An image inside the vacuum chamber with the farady cup aligned with the electron gun.

The high energy electron beam used in these experiments is a Kimball Physics EGPS-8105UD and is capable of generating electrons with energies up to 100 keV. For these experiments, the maximum beam energy used is 17 keV. In front of the cathode of the electron gun (the part that generates the electrons) is a grid that, when 500 V is applied to it, keeps all electrons from being emitted; they are not energetic enough to penetrate the electric field of the grid. If less

than 500 V is applied, some amount of electrons will escape the electron gun. By adjusting the voltage on this grid, the flux of electrons emitted from the beam can be controlled: the higher the grid voltage, the less electrons being emitted. To ensure the target is significantly encapsulated by the electron beam, the Faraday cup is aligned with the center of the electron gun aperture.

Three VUV lamps with wavelengths of 117 nm and 123 nm are used to excited photo-electrons from the target. The gold surface of the target object has a work function of 5.5 eV and the underlying copper has a work function of 4.1 eV[22]. With energies of 10.1 eV and 10.6 eV, the VUV photons are more energetic than the work functions and can excite electrons from the target surface. These lamps are not connected to the computer and can only be manually turned off and on; therefore, no control is applied to the VUV lights. An important note is that the VUV lamp configuration was not initially designed for active charge control experiments. Unlike the electron gun, none of the VUV lamps are directly aligned with target, meaning many of the photons do not impact the target.

As mentioned previously, the target object in these experiments is a gold plated copper disk. Secondary electron generation is a significant factor in charging experiments: they generate a positive current on the target surface that is difficult to account for because the secondary electron yield (SEY) is dependent on material properties and surface topology[1, 19, 20]. A copper disk was chosen as the target object, however copper oxidizes quickly in air, leading to a coating of copper oxide on the surface. The SEY of copper oxide is not well characterized. To account for this, the copper disk is sputter coated with a 100 nm gold layer, which has a much more thoroughly explored SEY. Figure 2 shows the total electron yield for poly-crystalline gold experimentally determined in Ref. 16. It is important to note that the second crossover point, E_2, occurs at 7 keV. As long as the landing energy of an electron is greater than E_2, the potential of a floating target will be driven to a value such that the landing energy is equal to E_2[1]. This means E_2 can be found by conducting floating potential experiments.

Due to size constraints of the sputter-coating machine, a uniform thickness of the gold coating is not guaranteed: the entire surface of the disk was plated with gold, but not uniformly 100 nm, however the minimum thickness will be 100 nm. While electrons will penetrate into the copper-oxide layer, the majority will be emitted from the gold layer. Ceramic standoffs and nylon screws are used to electrically isolate the disk from the rest of the setup. The target plate is connected outside the chamber via a high voltage feed-through (HFVT). This allows for the plate to be grounded and experiments to be reset after electron irradiation. Before being placed in the vacuum chamber, the target disk underwent a 16 hour 60^{o}C bake-out to remove additional impurities.

A Faraday cup and UV detector are included in the setup to measure the flux of electrons and VUV photons, respectively. Assuming the flux of the electrons is constant across the entire disk, the flux of electrons and photons impacting the plate can be approximated using these measurements. Care was taken to ensure the plate was not obstructing the aperture of the Faraday cup. With similar measurements, the flux of VUV photons impacting the target can be calculated as well. These measurements can then be used to explore the current balance and the secondary electron generation. During data collection, it was discovered that the UV detector measurements were effected by the electron beam. The outcome is that useful data of the VUV flux could not be collected while the electron beam was in use.

A Trek electrostatic voltmeter provides a contactless measurement of the target's potential. This probe functions as follows: the probe is placed roughly 3 mm from the target and, as the potential across the plate changes, the power supply drives the electric field between the target and the probe to zero, thereby achieving the same voltage on the probe as is on the plate. With a range of ± 20,000 volts and a resolution of 20 V, the Trek probe can accurately measure any potentials that are applied during these experiments. This probe can measurement at a rate of about 1 second, meaning the control applied here can be updated every second. Because the Trek probe is sensitive to electric fields, all metal (except for the disk) was grounded to reduce interference between the probe and the plate.

The equipment is controlled remotely through a LabView interface. This interface also applied the PD controller and processes/saves the experimental data collected by the instruments.

V. Experimental Results

A. Floating Potentials

The first step of the project is to determine the maximum floating potential that can be achieved by each beam energy. Throughout this paper, "floating potential" refers to the electrostatic potential applied to a target with an electron beam while it is isolated from ground or "floating". There may be some electron losses due to field electron emission, leakage currents, and coronal discharge from the HVFT, but these currents will be small compared to the electron beam current

and secondary electron current.

This characterization is used to support the choice of secondary electron yield model of the target as well as determine the maximum potential achievable for each beam energy. Figure 4 presents the relationship between the electron beam energy and floating potential for the given experimental setup. Between trials, the chamber is vented and

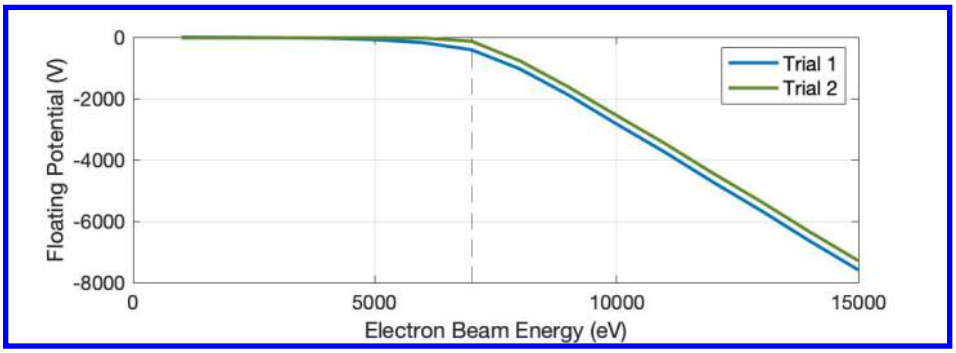

Fig. 4 The floating potential achieved by an electron beam with energies ranging from 1 keV to 16 keV. Both trials show a similar relationship, but with a -300 V offset for Trial 2.

.

the target is disconnected from the HVFT to test if there was significant coronal discharge from the end outside the chamber. When a highly charged object is exposed to atmosphere, if it has a strong electron field emission, the emitted electrons can ionize the surrounding atmosphere leading to a visible corona around the object. If coronal discharge is occurring, removing the HVFT would decrease the floating potential. From Fig. 4, it can be seen that both trials show the same relationship but with trial 2 shifted 283 V positive. The emission current from the electron gun is slightly less for trial 2, likely causing this difference, not coronal discharging. For both trials, until the beam energy reaches 6-7 keV, the target has a potentials comparable to the 20 V Trek probe resolution, meaning the object is not charging. Once the beam energy reaches 7 keV, the relationship between beam energy and floating potential becomes linear. From the linear sections, the average E_2 is estimated to be 7.3 keV. This is consistent with the SEY from Ref. 16 with a 4% error.

B. Proportional and Derivative Control Results

A PD controller, as described previously in section III, is developed in LabView for the active control throughout this project. Because the experimental setup is only capable of indirectly controlling the target potential, the output of the controller, is applied to the grid of the electron gun. When the goal potential is reached, the error is zero and the electron beam maintains a constant current such that the net flow of electrons into the target is zero. This control was applied to a variety of charging scenarios, with varying beam energies and goal potentials. Table 1 shows the charging behavior for the configurations that converged to steady state. This includes beam energies of 8 keV, 10 keV, and 12 keV and goal potentials ranging from -500 V to -4000 V. The following plots are shown for data collected using a 10 keV electron beam to achieve various goal potentials. Because the floating potential of the 10 keV beam is -2831 V, goal potentials up to this value can be achieved with this beam energy. If a larger potential is desired, the beam energy must

Table 1 Convergence behavior for multiple active charge control scenarios

Beam Energy (keV)	Goal Potential (V)	Time to Steady State (s)	Max Error at Steady State
8	-500	87	1.7%
8	-1000	116	0.6%
10	-500	90	2.4%
10	-1000	98	1.1%
10	-1500	106	0.7%
10	-2000	108	0.5%
12	-4000	72	0.2%

be increased. For all of the experiments presented in this section, the VUV lamps are on, applying a constant positive current to the target. It is also important to note that from 0 to about 40 seconds on Figs. 5-7 the target potential is zero. At the beginning of each trial, the grid potential starts at "Grid Cutoff", corresponding to a grid voltage of 500 V. Once the the control is applied, this grid voltage begins decreasing, but a measurable current is not emitted from the electron beam until the grid voltage reaches approximately 60 V (it varies slightly depending the electron beam energy). After the grid potential decreases below 60 V, charging occurs. This also means that at steady state, the grid voltage remains close to 60 V, oscillating sightly based on the target potential.

Fig. 5 shows the target potential as a function of time while the proportional and PD control is applied for a 10 keV beam driving the target to -500 V.

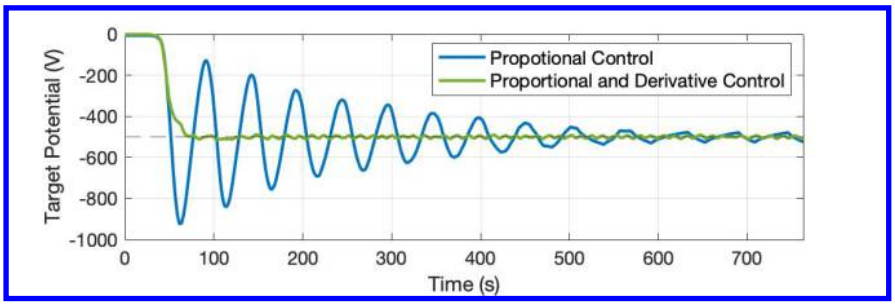

(a) Convergence behavior of both controllers over 750 seconds.

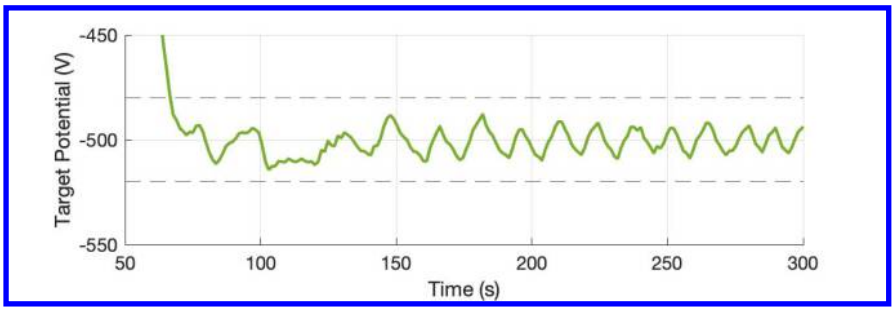

(b) Steady state behavior of the PD controller. A range of ± 20 V is shown by the dashed lines.

Fig. 5 The electric potential of the target as measured by the Trek probe for a 10 keV electron beam and a goal potential of -500 V.

From the top section of Fig. 5, it can be seen that both the P and PD control converge to the -500 V goal potential. The proportional control gives a smooth under-damped response that takes over 10 minutes to reach steady state behavior. Once it reaches the steady state, the target potential oscillates between -480 V and -526 V, giving a maximum deviation of 26 V or 5.2%. Including the derivative control results in a slightly over-damped system. The target charges to the -500 V goal in 90 seconds and almost immediately enters the steady state behavior with the potential oscillating between -488 V and -510 V. This corresponds to a maximum deviation of 2.4%. By incorporating derivative control, the goal potential is achieved in 15% of the time and the maximum residual is cut in half compared to just proportional control. All of this behavior is dependent on the gains chosen for the system. For the data in Fig. 5, the proportional gain is chosen to 0.0018 and the derivative gain is chosen to be 18.5. These gains are chosen because they yield the fastest convergence time with small deviations at steady state.

Similar results were found for the other charging scenarios as well. Figure 6 shows the data collected for a 10 keV beam achieving a -1500 V potential on the target object.

Again it can be seen that the proportional control has a similar under-damped behavior that converges after about 10 minutes. The steady state residuals are slightly large with a maximum deviation of 31 V. It is more interesting to examine the PD control. First, at 50 seconds, the potential begins to increase even though the target has not reached the goal potential. This indicates that derivative gain is too large: the controller registers the rate of change of the target potential as too large and decreases the electron beam current to account for this. Second, the system is also slightly under-damped. This occurs because the proportional gain is too high and the derivative control does not counter it as the target potential approaches -1500 V. Despite this, steady state behavior is reached after 106 s and the maximum

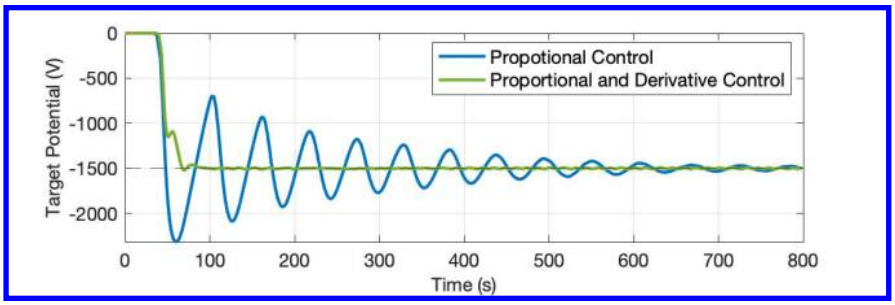

(a) Convergence behavior of both controllers over 800 seconds.

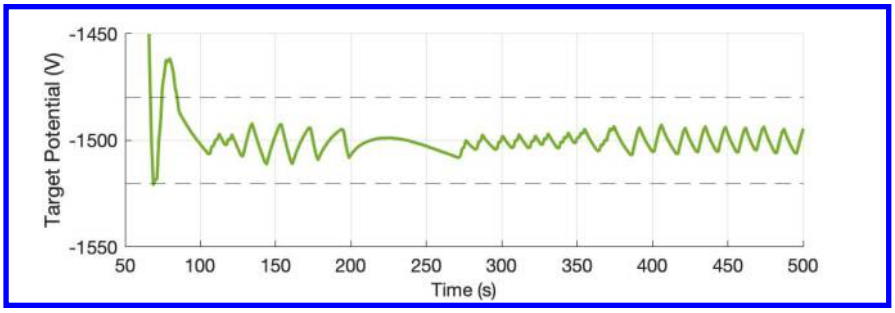

(b) Steady state behavior of the PD controller. A range of ± 20 V is shown by the dashed lines.

Fig. 6 The charging behavior of the target for a 10 keV electron beam and a goal potential of -1500 V.

deviation from the goal is 11 V, corresponding to a 0.7% error.

Figure 7 shows the behavior of a system with a goal potential of -2000 V and a beam energy of 10 keV.

Similar to Fig. 6, the derivative gain is slightly too high and at 55 s the current begins to increase even though the target potential is only -1755 V. However, steady state potential is still achieved in 108 s with a max error of 0.5% (10 V). Comparing the previous three charging plots, there are some trends that can be seen emerging. As the goal potential increases, the time it takes to reach the goal, and steady state, increases. Even the under-damped system in Fig. 6 converges faster than the slightly over-damped system of Fig. 7. From Table 1, this behavior can be seen for each of the 10 keV trials and the 8 keV trials. This is expected because the target always starts at 0 V, meaning the larger goal, the more "distance" needs to be traveled. The rate of charging can be increased by increasing the proportional gain, but that leads to under-damped behavior, increasing the time to steady state.

The other trend is that for each of the 10 keV trials, the maximum residual remains about 10 V. Each set of gains is selected because they result in the least amount of time to reach steady state. Different gains could be found such that the system is critically damped and the time to convergence is minimized, however the results shown here should be close to this critically damped system. This suggests that, when the system is close to being critically damped, the error at steady state is relatively constant across a range of goal energies for a given beam energy. Only two trials at 8 keV where conducted but the maximum residuals where approximately 8 V and 6 V, which, while not identical, are still very close in size. More experiments would need to be conducted to confirm this.

One trend that is not demonstrated by the figures or table is that for a given beam energy, as the goal potential increases, the gains become less sensitive: it takes larger changes in the gains to get noticeable changes to the charging behavior. This likely due to the fact that, as the target potential approaches the floating potential, the amount of current reaching the target decreases. At the floating potential, the net current experienced by the target is 0 because the incoming and outgoing currents are equal[1]. At values close to the floating potential, the net current is small and the ratio of incoming electrons to outgoing electrons is close to 1. Increasing the electron beam current would have less of an effect because the incoming and outgoing electron currents would still be similar, leading to less sensitive control. Conversely, when the target potential is not close to the floating potential, the incoming current will be greater than the outgoing current. In this case, increasing the beam current would have a more significant effect on the target potential, leading to more sensitive control.

One consequence of this is that it becomes extremely difficult to achieve small goal potentials using large beam energies. This was explored by attempting to achieve a -500 V potential with a beam energy of 15 keV. Over the

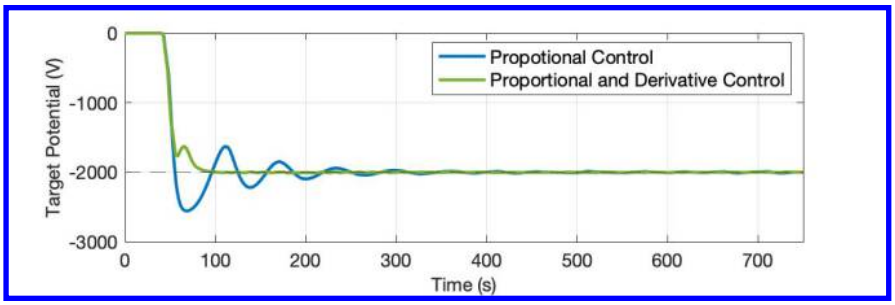

(a) Convergence behavior of both controllers over 750 seconds.

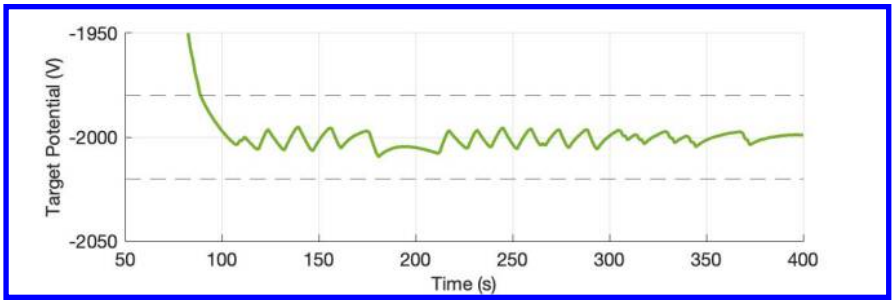

(b) Steady state behavior of the PD controller. A range of ± 20 V is shown by the dashed lines.

Fig. 7 The charging behavior of the target for a 10 keV electron beam and a goal potential of -2000 V.

course of many iterations and gain configurations a control could not be achieved that converged the -500 V and had a reasonable error at steady state: the system was too sensitive to δV. Some gains did lead to convergence, however, the target potential would oscillate around - 500 V with amplitudes greater than 100 V: far too big of an error. While this does not prove there is no gain configuration that would achieve this control, it does show that using large beam energies will lead to difficulties achieving small goal potentials. This may be accounted for by implementing electron beam energy control as well as current control. A discussion of this type of control will be presented later.

C. Discharging Behavior Using a Photo-Electric Current

An important aspect of these charging scenarios is the discharging. Up until this point, the VUV lamps have been on. These VUV lights have two major purposes: discharge the target quickly and allow the target to charge slightly positive. This is achieved through the induced photo-electric effect: high energy photons impact the target and may be absorbed by the surface electrons. If the energy of the photon is greater than the work function of the material, the electron will be emitted from the target. These electrons are emitted with small energies (less than 1-3 eV)[23]. When the target has a negative potential, the emitted electron will be repelled from the target, resulting in a positive current. This is allows a negatively charged target to discharge quickly when the electron beam current is zero. With this constant positive current, the target object will eventually charge positive. A positively charged target will attract the low energy photo-electrons back, leading to a weakly positive charge on the target.

For ground testing, including these VUV lamps is relatively simple; the size, weight, and power requirements are easy to overcome. However, incorporating them onto a spacecraft mission will take away from the SWaP budget, therefore it is important to explore the necessity of this photo-electron current for active charge control. Figure 8 compares the discharging behavior with and without the VUV lights. Without this photo-electric current, the only positive currents on the target are the leakage current through the ceramic stand-off, field emission from the high charge density areas, and impacts from the small number ions present in the chamber. These currents are small compared to the photo-electric current of the VUV lights and this can be seen in the remarkable difference in discharging times shown in Fig. 8. With the VUV lights on, the target fully discharges from -4000 V in 130 seconds. Without the VUV lights, it takes over an hour to discharge 3800 V: 29 times longer and the target does not fully discharge.

As stated previously, it is expected that the target should charge a few volts positive because of the photo-electric effect and Fig. 8 shows that the target only reaches -3 V. The final potential is not slightly positive as expected. This is due to the 20 V resolution of the electrostatic voltage: the final potential will be within ± 20 V of -3 V, which includes

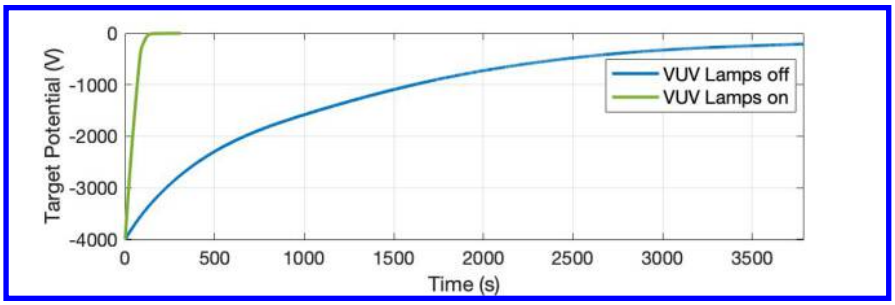

(a) Discharging behavior over the course of 1 hour.

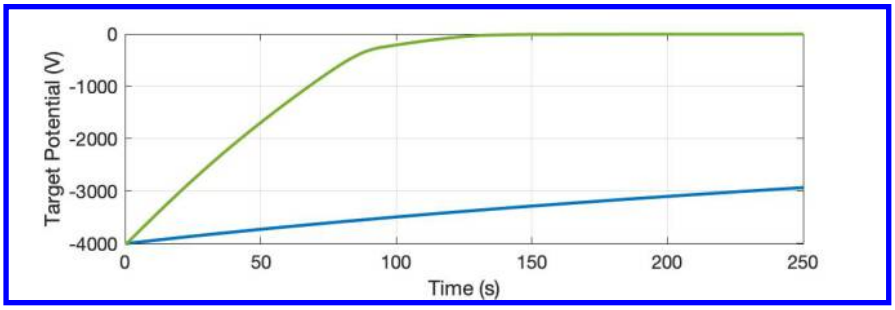

(b) Discharging behavior over the course of 250 seconds.

Fig. 8 Discharging of a target with a -4000 V potential with and without the photo-electric current.

slightly positive values. To confirm that the target is positively charged, a voltmeter with better resolution would be required.

The significant increase in charging times without VUV lights leads to control that is extremely sensitive to under-damped systems because any overshoot takes a significant amount of time to discharge back to the goal potential. Figure 9 compares the charging behavior of the PD controller for an 8 keV and 10 keV beam achieving a goal potential of -500 V with and without the photo-electric effect. In both cases, without the VUV lights, the control overshoots the goal potential and has to slowly discharge. With an 8 keV electron beam, the target exceeds the goal potential by 74 V. After 181 seconds, the target discharges to -533, still a significant deviation. In contrast, the control with the VUV lights has been in steady state for nearly 200 seconds.

A similar result is seen for the 10 keV electron beam: without the VUV lamps, the target charges to -608 V and discharges to -541 V after 315 seconds. As shown, the first oscillation lasts more than a couple of minutes, and waiting for this control to possibly converge takes significantly more time. These results suggest that, for the system to converge in a realistic amount of time, this photo-electric effect must be applied, therefore VUV lamps are necessary for active charge control. The next section, however, explores the use of electron beams for discharging and how that effects the VUV lamp requirement.

D. Discharging Behavior Using the Electron Beam

Experimenting with electron beam energies led to the discovery that the electron beam can be used to discharge the target object. Initially, this appears counter intuitive: the electron beam is a negative current and one would not expect it to increase the potential of a target. However, because the secondary electron emission drives the target to the second crossover point, this can be an effective method of discharging. If a target's potential is -8000 V and a 9 keV electron is directed at it, the potential will be driven to rapidly to -1882 V (or something close), the floating potential for a 9 keV beam. Figure 10 shows the discharging of a -8300 V target using different electron beam energies.

Over the 50 second sample time, three discharging behaviors can be seen. For the 9 keV beam, the target is quickly driven to -1844 V. Beam energies of 1 keV and 3 keV discharge slowly and do not reach the associated floating potentials. The interesting behavior can be seen for the 5 keV and 7 keV beams. Initially, the target discharges similar to the 1 keV and 3 keV beams. After the target potential reaches a certain value, it decreases rapidly, similar the effect of the 9 keV beam. This behavior occurs because when the target potential is greater (more negative) than the beam energy, the

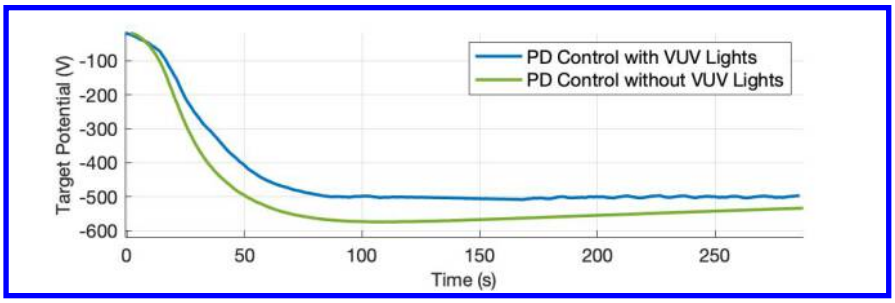

(a) Convergence behavior of an 8 keV electron beam.

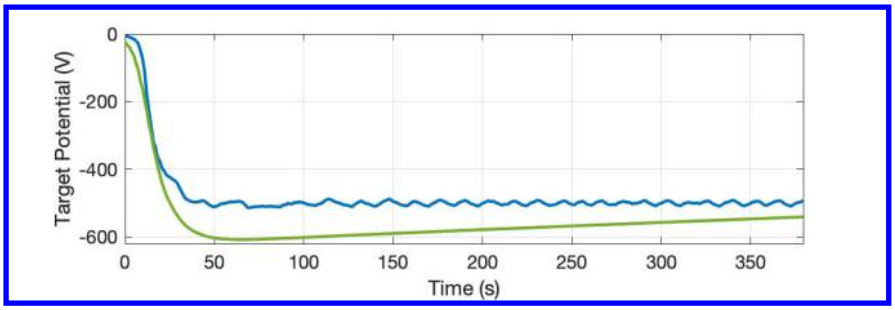

(b) Convergence behavior of a 10 keV electron beam.

Fig. 9 A comparison of charging behavior for different beam energies and a goal potential of -500 V with and without VUV lights.

electron beam electrons do not have enough energy to penetrate the electric field of the target; they are deflected and do not impact the plate. Once the target potential drops below the beam energy, the electrons can impact the target and secondary electrons drive the potential to the floating potential value. Figure 10 shows this clearly for 7 keV: once the target potential reaches -7097 V, it is quickly driven to -425 V, close to the respective floating potential. The same behavior is also seen for the 5 keV beam energy. These results demonstrate that an electron beam can be used to

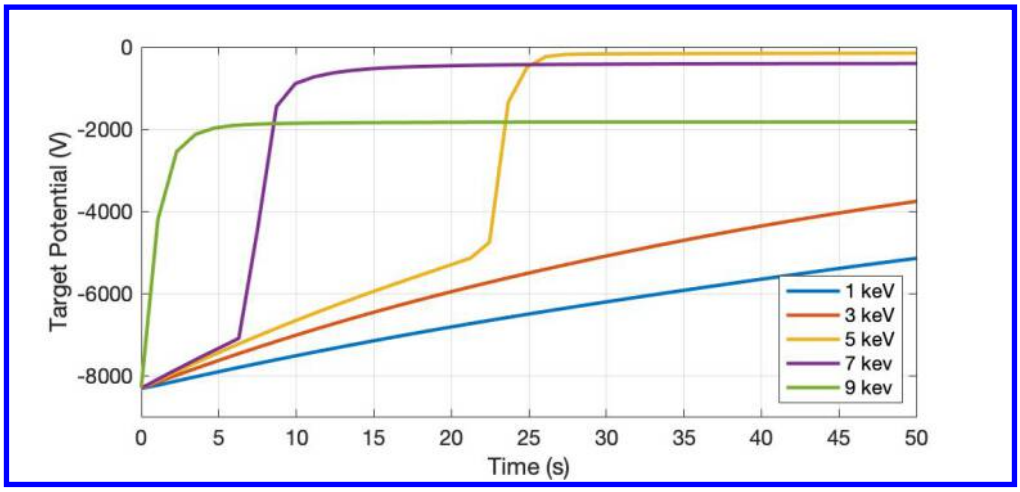

Fig. 10 Discharging a target using an electron beam for various beam energies.

discharge a target which calls into the question the requirement of the VUV lights. In order to use the electron beam for charging and discharging, control must applied to the beam energy. This control was also brought up previously with the discovery that large electron beam energies could converge to low goal potentials. To account for this, the PD controller could be applied to the beam energy rather than the grid: if the target potential is too low/high, the control would increase/decrease the beam energy by δV. When the goal potential is achieved, δV = 0, so the beam energy

will remain constant. With this control, the system could achieve any goal potential (as long as it is not larger than the capability of the electron gun) and the goal potential would be close to the floating potential of the beam energy, meaning the controller would have a low sensitivity.

The electron beam could also be used to fully discharge the target object. A beam energy slightly greater than the target potential could be directed at the target. This would quickly drive the value to the floating potential. This process would repeat until the object is fully discharged. For example, if the target object has a potential of -8500 V, a 9 keV electron beam would drive the potential to -1882 V. Next, the beam energy would be adjusted to 2 keV, which would then drive the target potential to near 0 V. Exploring electron beam energy control would be a logical next step for this research.

VI. Conclusion

The main objective of this paper is to develop active charge control using an electron beam. For a variety of beam energies, the electron gun with a PD beam current control is able to drive a target object to a goal potential and maintain steady state behavior with less than 2.5% error across all presented scenarios. In some cases, less than 1% deviation from the goal potential is achieved. These results demonstrate that active charge control is achieved in vacuum chamber conditions.

Discharging behavior is also explored with the purpose of justifying the inclusion of the additional VUV lamps. The results show that in order to have realistic convergence times, a method for discharging the circuit must be implemented, in this case, the positive photo-electric current generated by the VUV lamps allow the target to discharge rapidly. Additionally, they allow for the target to be charged slightly positive. This is beneficial specifically for reducing electrostatic torques and forces during docking and proximity operations. Using the VUV lamps, the spacecraft potentials can be driven to near zero values. The Coulomb forces are directly proportional to the charge on the spacecraft, therefore near zero potentials results in near zero forces. This also reduces the risk of ESD during docking: if both spacecraft have slightly positive values, there is not a large enough potential difference for arching to occur.

During the course of this paper, it was discovered that the electron gun can be used to discharge the target object, which may eliminate the need for VUV lamps. This requires the control be applied to the electron beam energy rather than the current. One drawback, however, is that this type control cannot be used to eliminate electrostatic forces or ESD events. To discharge using just the electron gun, the servicing spacecraft needs to constantly be emitting electrons, meaning the potential will positively increase proportionally to the electron beam energy. Because the target potential is small the Coulomb forces are reduced, but still present. Also, during docking, there would be a significant potential difference between the two spacecraft which increases the probability of damaging ESD events.

Acknowledgments

A special thanks to Ryan Hoffmann and the Spacecraft Charging and Instrument Calibration Lab at the Air Force Research Laboratory for the use of their facilities and assistance with this research.

References

[1] Lai, S. T., *Fundamentals of Spacecraft Charging*, Princeton University Press, 2011. https://doi.org/10.2307/j.ctvcm4j2n.

[2] Wilson, K., and Schaub, H., "Impact of Electrostatic Perturbations on Proximity Operations in High Earth Orbits," *Journal of Spacecraft and Rockets*, Vol. 58, No. 5, 2021, pp. 1–10. https://doi.org/10.2514/1.a35039.

[3] Wilson, K., and Schaub, H., "Constrained guidance for spacecraft proximity operations under electrostatic perturbations," *IEEE Aerospace Engineering Conference*, Big Sky, MT, 2021, pp. 1–11.

[4] Wilson, K. T. H., 'Alvaro Romero Calvo, and Schaub, H., "Constrained Guidance for Spacecraft Proximity Operations Under Electrostatic Perturbations," *Journal of Spacecraft and Rockets*, Vol. 59, No. 4, 2022, pp. 1304–1316. https://doi.org/10.2514/1.A35162.

[5] Schaub, H., and Moorer, D. F., "Geosynchronous Large Debris Reorbiter: Challenges and Prospects," *The Journal of the Astronautical Sciences*, Vol. 59, No. 1-2, 2012, pp. 161–176. https://doi.org/10.1007/s40295-013-0011-8.

[6] Schaub, H., and Sternovsky, Z., "Active Space Debris Charging for Contactless Electrostatic Disposal Maneuvers," *Advances in Space Research*, Vol. 43, No. 1, 2014, pp. 110–118. https://doi.org/dx.doi.org/10.1016/j.asr.2013.10.003.

[7] Moorer, D. F., and Schaub, H., "Electrostatic spacecraft reorbiter," , 2011a.

[8] Moorer, D. F., and Schaub, H., "Hybrid electrostatic space tug," , 2011b.

[9] Schaub, H., and Jasper, L. E. Z., "Circular Orbit Radius Control Using Electrostatic Actuation for 2-Craft Configurations," *AAS/AIAA Astrodynamics Specialist Conference*, Girdwood, Alaska, 2011. Paper AAS 11–498.

[10] Pedersen, A., Chapell, C., Knott, K., and et all, "Methods for keeping a conductive spacecraft near the plasma potential," *Spacecraft Plasma Interactions and Their Influence on Field and Particle Measurements, Proceedings of the 17th ESLAB Symposium, ESA SP-198*, Citeseer, 1983, pp. 185–190.

[11] Schmidt, R., Arends, H., Torkar, K., and Valanvanoglou, N., *Novel Methods for Active Spacecraft Potential Control*, American Geophysical Union (AGU), 1989, pp. 261–265. https://doi.org/https://doi.org/10.1029/GM054p0261.

[12] Schmidt, R., Arends, H., Pedersen, A., Rüdenauer, F., and et al, "Results from Active Spacecraft Potential Control on the Geotail Spacecraft," *Journal of Geophysical Research: Space Physics*, Vol. 100, No. A9, 1996, pp. 17253–17259. https://doi.org/https://doi.org/10.1029/95JA01552.

[13] Torkar, K., Riedler, W., Escoubet, C. P., and et al, "Active Spacecraft Potential Control for Cluster – Implementation and First Results," *Ann. Geophys.*, 2001. https://doi.org/https://doi.org/10.5194/angeo-19-1289-2001.

[14] Torkar, K., Nakamura, R., and Tajmar, M., "Active Spacecraft Potential Control Investigation," *Space Sci Rev*, 2016. https://doi.org/10.1007/s11214-014-0049-3.

[15] Schaub, H., Parker, G. G., and King, L. B., "Challenges and Prospect of Coulomb Formations," *Journal of the Astronautical Sciences*, Vol. 52, No. 1–2, 2004, pp. 169–193.

[16] Hoffmann, R. C., "Electron-Induced Electron Yields of Uncharged Insulating Materials," Master's thesis, Utah State University, 2010. https://doi.org/https://doi.org/10.26076/1e55-9dc9.

[17] Hammerl, J., Haft, A., and Schaub, H., "Neighboring Spacecraft Charging due to Continuous Electron Beam Emission and Impact," *Applied Space Environments Conference*, 2023.

[18] Lundgreen, P., and Dennison, J. R., "Strategies for Determining Electron Yield Material Parameters for Spacecraft Charge Modeling," *Space Weather*, Vol. 18, No. 4, 2020. https://doi.org/https://doi.org/10.1029/2019SW002346.

[19] Lundgreen, P., and Dennison, J. R., "Strategies for Determining Electron Yield Material Parameters for Spacecraft Charge Modeling," *Space Weather*, Vol. 18, No. 4, 2020, p. e2019SW002346. https://doi.org/https://doi.org/10.1029/2019SW002346.

[20] Baglin, V., Bojko, J., Gröbner, O., Henrist, B., Hilleret, N., Scheuerlein, C., and Taborelli, M., "The Secondary Electron Yield of Technical Materials and its Variation with Surface Treatments," 2000.

[21] Walker, J., Hammerl, J., and Schaub, H., "Experimentally Estimating Secondary Electron Yield," *Applied Space Environments Conference*, 2023.

[22] Hayes, W. M., *CRC Handbook of Chemistry and Physics*, 95$^{\text{th}}$ ed., CRC Press, 2014.

[23] Lai, S., and Tautz, M., "Aspects of Spacecraft Charging in Sunlight," *IEEE Transactions on Plasma Science*, Vol. 34, No. 5, 2006, pp. 2053–2061. https://doi.org/10.1109/TPS.2006.883362.